

1   **Explicit modelling of isoprene chemical processing in polluted air**  
2   **masses in suburban areas of the Yangtze River Delta region:**  
3   **radical cycling and formation of ozone and formaldehyde**  
4

5   **Kun Zhang<sup>a, b</sup>, Ling Huang<sup>a, b</sup>, Qing Li<sup>a, b</sup>, Juntao Huo<sup>c</sup>, Yusen Duan<sup>c</sup>, Yuhang Wang<sup>d</sup>, Elly**  
6   **Yaluk<sup>a, b</sup>, Yangjun Wang<sup>a, b</sup>, Qingyan Fu<sup>c</sup>, Li Li<sup>a, b\*</sup>**

7   <sup>a</sup> School of Environmental and Chemical Engineering, Shanghai University, Shanghai, 200444, China

8   <sup>b</sup> Key Laboratory of Organic Compound Pollution Control Engineering, Shanghai University, Shanghai,  
9   200444, China

10   <sup>c</sup> Shanghai Environmental Monitoring Center, Shanghai, 200235, China

11   <sup>d</sup> School of Earth and Atmospheric Sciences, Georgia Institute of Technology, Atlanta, GA, USA

12   *Correspondence to Li Li (Lily@shu.edu.cn)*

13

14   **Abstract**

15   In recent years, ozone pollution has become among the most severe environmental  
16   problems in China. Evidence from observations have showed increased frequency of high O<sub>3</sub>  
17   levels in suburban areas of the Yangtze River Delta (YRD) region. To better understand the  
18   formation mechanism of local O<sub>3</sub> pollution and investigate the potential role of isoprene  
19   chemistry in the budgets of ROx (OH+HO<sub>2</sub>+RO<sub>2</sub>) radicals, synchronous observations of  
20   volatile organic compounds (VOCs), formaldehyde (HCHO) and meteorological parameters  
21   were conducted at a suburban site of the YRD region in 2018. Five episodes with elevated O<sub>3</sub>  
22   concentrations under stagnant meteorological conditions were identified; an observation-based  
23   model (OBM) with the Master Chemical Mechanism was applied to analyze the photochemical  
24   processes during these high O<sub>3</sub> episodes. The high levels of O<sub>3</sub>, nitrogen oxides (NOx), and  
25   VOCs facilitated strong production and recycling of ROx radicals with the photolysis of

26 oxygenated VOCs (OVOCs) being the primary source. Our results suggest that, local biogenic  
27 isoprene is important in suburban photochemical processes. Removing isoprene could  
28 drastically slow down the efficiency of ROx recycling and reduce the concentrations of ROx.  
29 Besides, the absence of isoprene chemistry could further lead to decrease in the daily average  
30 concentration of O<sub>3</sub> and HCHO by 34% and 36%, respectively. Therefore, this study  
31 emphasizes the importance of isoprene chemistry in suburban atmosphere, particularly with  
32 the participation of anthropogenic NOx. Moreover, our results provide insights into the radical  
33 chemistry that essentially drives the formation of secondary pollutants (e.g. O<sub>3</sub> and HCHO) in  
34 the suburban of YRD region.

35 **Keywords:** Isoprene; Observation-based model (OBM); Radical; Ozone; Yangtze River Delta

## 36 1. Introduction

37 The hydroxyl radical (OH), hydro peroxy radical (HO<sub>2</sub>) and organic peroxy radical (RO<sub>2</sub>),  
38 collectively known as ROx dominate the oxidative capacity of the atmosphere and hence  
39 govern the removal of primary contaminants (e.g. volatile organic compounds (VOCs)) and  
40 the formation of secondary pollutants (e.g. ozone (O<sub>3</sub>), secondary organic aerosols (SOAs))  
41 (Liu et al., 2012; Xue et al., 2016). ROx radicals can undergo efficient recycling (e.g. OH→  
42 RO<sub>2</sub>→RO→HO<sub>2</sub>→OH) and produce O<sub>3</sub> and oxygenated VOCs (OVOCs) (Liu et al., 2012;  
43 Tan et al., 2019; Xue et al., 2016). In addition, the photolysis of OVOCs can in turn produce  
44 primary RO<sub>2</sub> and HO<sub>2</sub> radicals, and further accelerate the recycling of ROx (Liu et al., 2012).  
45 The reaction rates of different VOCs with ROx vary significantly (Atkinson and Arey, 2003;  
46 Atkinson et al., 2006). For instance, the reaction rate constants for OH with ethane and ethene  
47 are  $0.248 \times 10^{-12}$  (cm molecule<sup>-1</sup> s<sup>-1</sup>) and  $8.52 \times 10^{-12}$  (cm molecule<sup>-1</sup> s<sup>-1</sup>), respectively. Among  
48 the hundreds and thousands of VOC species, isoprene (C<sub>5</sub>H<sub>8</sub>, 2-methyl-1,3-butadiene) is  
49 among the most active and abundant biogenic VOCs (BVOCs) species globally (Wennberg et

50 al., 2018). Over the past decades, isoprene emission sources have been extensively studied  
51 (Gong et al., 2018) and recent works have focused on the degradation pathways and the impact  
52 of isoprene chemistry on regional forest chemistry (Gong et al., 2018; Wolfe et al., 2016a).  
53 Previous studies showed that isoprene could be quickly oxidized by atmospheric oxidants (e.g.  
54 OH, O<sub>3</sub> or NO<sub>3</sub>) (Wolfe et al., 2016a; Gong et al., 2018; Jenkin et al., 2015). Due to the rapid  
55 reaction between OH and isoprene ( $100 \times 10^{-12}$  cm<sup>3</sup> molecule<sup>-1</sup> s<sup>-1</sup> at 298 K), more than 90% of  
56 the total daytime isoprene is removed via this reaction (Wennberg et al., 2018). The reaction  
57 between OH and isoprene is initiated by the addition of OH and can generate isoprene  
58 hydroxyperoxy radicals (ISOPO<sub>2</sub>) (Wennberg et al., 2018; D'Ambro et al., 2017; Liu et al.,  
59 2013; Jenkin et al., 2015). ISOPO<sub>2</sub> isomers could then interconvert rapidly due to reversible  
60 O<sub>2</sub> addition and are finally removed via reactions with HO<sub>2</sub> or NO (Jenkin et al., 2015; Wolfe  
61 et al., 2016a). Hence, the degradation process of isoprene is tightly associated with RO<sub>x</sub>  
62 recycling. According to He et al. (2019), isoprene chemistry could strongly influence the  
63 photochemical formation of O<sub>3</sub>, with a relative incremental reactivity (RIR) of ~0.06%/%.  
64 Besides, HCHO is also formed via several pathways during the depletion of isoprene (Jenkin  
65 et al., 2015; Wolfe et al., 2016a) and is found to be highly sensitive to isoprene emissions (Zeng  
66 et al., 2019).

67 The Yangtze River Delta (YRD) region is one of the most developed city-clusters in  
68 eastern China and is under serious O<sub>3</sub> pollution (Zhang et al., 2019; Zhang et al., 2020a; Chan  
69 et al., 2017). At the suburban area of YRD, high levels of O<sub>3</sub> have been frequently observed  
70 (Zhang et al., 2019; Zhang et al., 2020a). Several studies have investigated the relationship  
71 between O<sub>3</sub> and its precursors (Chan et al., 2017; Lin et al., 2020; Zhang et al., 2020a; Zhang  
72 et al., 2020b), but few studies have addressed the atmospheric oxidizing capacity and radical  
73 chemistry involved in these complicated photochemical processes (Tan et al., 2019; Zhu et al.,  
74 2020b). Previous studies have pointed out that the high levels of O<sub>3</sub> at suburban areas of

75 Shanghai could be attributed to the transport of O<sub>3</sub> or its precursors from urban areas (Lin et  
76 al., 2020; Zhang et al., 2019; Li et al., 2016; Li et al., 2019). On the contrary, high O<sub>3</sub>  
77 concentrations were frequently observed in suburban areas under stable meteorological  
78 conditions. Therefore, given the dense vegetation cover in suburban YRD and weak transport  
79 of air masses, the importance of local isoprene chemistry regarding ozone formation remains  
80 unclear.

81 In this study, we conducted a comprehensive set of in-situ observations of isoprene  
82 concentration, meteorological conditions, and concentrations of atmospheric pollutants  
83 (including O<sub>3</sub>, NO<sub>x</sub>, CO, VOCs, and HCHO) to understand the impact of isoprene chemistry  
84 on atmospheric photochemical processes in suburban YRD region. We used an observation-  
85 based model (OBM) to explore the role of local isoprene chemistry in radical budgets and the  
86 formation of O<sub>3</sub> and HCHO. Results from this study provides insights into the isoprene  
87 chemistry in the suburban region of a fast-developing city-cluster.

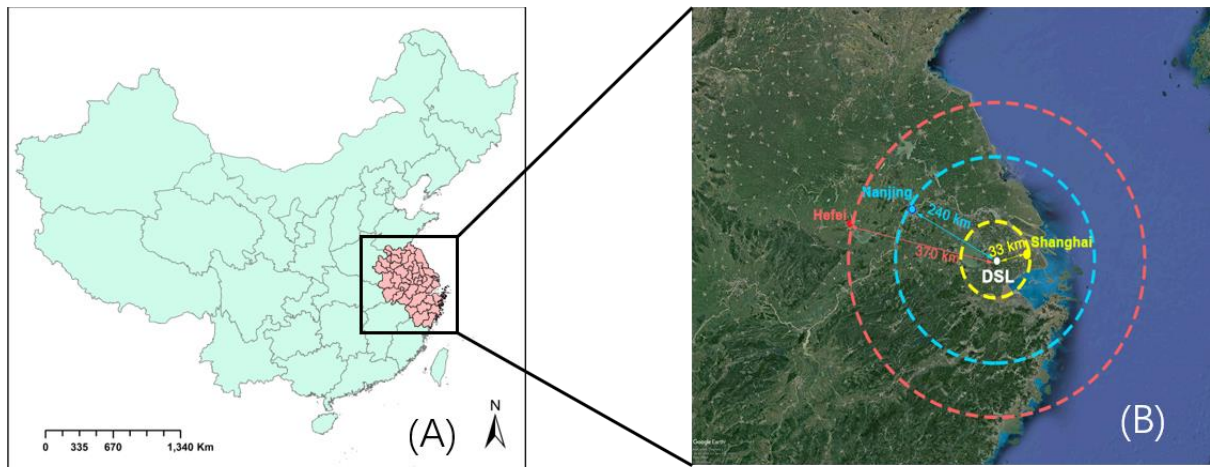
## 88 **2. Methodology**

### 89 **2.1 Field measurement**

90 The observations were conducted at a supersite (120.98°E, 31.09°N) in the suburban areas  
91 of the YRD region (Figure 1). It is located in the west of Shanghai and is close to the Dianshan  
92 Lake Scenic area, with relatively higher vegetation cover than the urban areas. To investigate  
93 the local isoprene chemistry and its influence on O<sub>3</sub> and HCHO formation, continuous  
94 measurements were conducted from April 7<sup>th</sup> to September 25<sup>th</sup>, 2018, when photochemical  
95 activity and O<sub>3</sub> formation is significant.

96

97



98

99 **Figure 1.** (A) map of China with YRD region highlighted in pink; and (B) satellite map of YRD region  
100 (created with Google Earth© on 23<sup>rd</sup> July 2020).

101 **Table 1. Measurements performed during the ozone season.**

Species/Parameter	Experimental Technique	Time resolution	Lower Detectable limit
O <sub>3</sub>	Model 49i, Thermo Fischer Scientific, USA	60 s	0.5 ppbv
NO and NO <sub>2</sub>	Model 42i, Thermo Fischer Scientific, USA	60 s	0.4 ppbv
CO	Model 48i, Thermo Fischer Scientific, USA	60 s	40 ppbv
HCHO	AL4021, Aero-Laser, GER	90 s	0.1 ppbv
VOCs species	GC866, Agilent., USA	1 hour	-
Temperature, relative humidity, wind speed and wind direction	Meteorological station, Vaisala, FIN	60 s	-

102

103 The measuring instruments are shown in Table 1. Wind speed (WS), wind direction (WD),  
104 ambient pressure (P), temperature (T), and relative humidity (RH) were simultaneously  
105 observed by a meteorological station (Vaisala., FIN). According to China's air quality standard,  
106 several criteria air pollutants were measured during this experiment. For instance, O<sub>3</sub> was  
107 measured by an ultraviolet photometric analyzer (Model 49i, Thermo Fischer Scientific., USA),  
108 with a detection limit of 0.5ppbv, whereas nitrogen oxides (NO and NO<sub>2</sub>) were simultaneously  
109 observed by a chemiluminescence instrument (Model 42i, Thermo Fischer Scientific., USA),  
110 with a detection limit of 0.4ppbv. Likewise, carbon monoxide (CO) was monitored by a gas  
111 filter correlation infrared absorption analyzer (Model 48i, Thermo Fischer Scientific., USA),  
112 with a detection limit of 0.04ppm. All the online instruments used for gas analyzer were auto-

113 zero every day, and were multi-point calibrated every month. All the instruments used for the  
114 online observation were housed on top of a 5-floor-high building, which was about 15 m above  
115 the ground level.

116 A total of 55 VOC species, including 28 alkanes, 10 alkenes (including isoprene), 16  
117 aromatics and acetylene were continuously analyzed at our sampling site by two online gas  
118 chromatographs with flame ionization detector (GC-FID) systems (GC-866 airmoVOC C<sub>2</sub>-C<sub>6</sub>  
119 #58850712 and airmoVOC C<sub>6</sub>-C<sub>12</sub> #283607112, Agilent., USA) with a time resolution of 1  
120 hour during the study period. Ambient samples are directly inhaled into this system by a pump.  
121 Low carbon VOCs (C<sub>2</sub>-C<sub>6</sub>) are captured by a low temperature (-10 °C) pre-concentration  
122 system, while high carbon VOCs are concentrated by a built-in room temperature pre-  
123 concentration system. Then the preconcentration system are heated and desorb VOCs, which  
124 are eventually carried into the chromatographic columns by helium. Individual VOCs separated  
125 in the columns are eventually detected by FID systems. Formaldehyde (HCHO) was  
126 continuously measured by a Hantzsch fluorescence technique (AL4201, Aerolaser GmbH.,  
127 GER), which is based on fluorometric Hantzsch reaction in the liquid phase, requiring the  
128 quantitative transfer of HCHO from gas phase to liquid phase. A Hantzsch reagent  
129 (acetylacetone) was used in this instrument.

130 **2.2 Observation-based model**

131 In this study, a zero-dimensional (0-D) box model (F0AM) (Wolfe et al., 2016b) based on  
132 the University of Washington Chemical Model (UWCM) was used to simulate the atmospheric  
133 chemical processes. Dry deposition and atmospheric dilution were considered in this model.  
134 The Master Chemical Mechanism (MCM) v3.3.1 with more than 5,800 chemical species and  
135 17,000 reactions was used in this study to enable a detailed description of the complex  
136 chemical reactions. In addition to gas-phase reactions, several heterogeneous processes  
137 including the uptake of HO<sub>2</sub>, N<sub>2</sub>O<sub>5</sub> and HCHO on aerosol surface as well as heterogeneous

138 sources of nitrous acid (HONO) were considered in our simulation. The rate constants and  
 139 uptake coefficient of these reactions were obtained from the study of Riedel et al. (2014), Xue  
 140 et al. (2014) and Li et al. (2014). Since key parameters such as aerosol surface area ( $S_A$ ) and  
 141 particle diameter ( $r$ ) were not measured, an average  $S_A$  ( $640 \text{ nm}^2/\text{cm}^3$ ) was adopted from the  
 142 field campaign in Shanghai (Wang et al., (2014)).

143 **Table 2. Heterogenous reactions and associated rate constants used in the OBM model.**

Reactions	Reaction rate constant	Reference
$N_2O_5 \rightarrow CLNO_2 + HNO_3$	$\gamma\omega S_A/4$ (for $CLNO_2$ formation) $(2 - \phi)\gamma\omega S_A/4$ (for $HNO_3$ formation)	Riedel et al. (2014)
$NO_2 \rightarrow HONO$	$k_g = \frac{1}{8} \times \omega \gamma_g \left(\frac{S}{V}\right)$	Xue et al. (2014)
$HO_2 \rightarrow products$	$k = \left(\frac{r}{D_g} \frac{4}{\gamma} \omega\right)^{-1} S_A$	Xue et al. (2014)
$HCHO \rightarrow products$	$k = \frac{1}{4} \omega \gamma S_A$	Li et al. (2014)

$\gamma$ = uptake coefficient for the given reactant with aerosol surface area;  $\phi$  = product yield;  $\omega$ =mean molecular speed of the given reactant (m/s);  $S_A$ =RH corrected aerosol surface area concentration ( $\text{nm}^2/\text{cm}^3$ );  $r$ =surface-weighted particle radius.

144  
 145 Photolysis frequencies ( $J$  values) were calculated by a trigonometric parameterization  
 146 based on solar zenith angle (SZA):

$$J = I \cos(SZA)^m \exp(-n \sec(SZA)) \quad (1)$$

147 where  $I$ ,  $m$  and  $n$  are constants unique to each photolysis reaction, derived from least-  
 148 squares fits to  $J$  values computed with fixed solar spectra and literature cross-section and  
 149 quantum yields (Wolfe et al., 2016b). Hourly average concentrations of speciated VOCs  
 150 (except HCHO), NO,  $NO_2$ , CO and meteorological parameters (such as T, RH and P) were

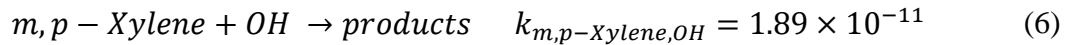
151 used to constrain the F0AM model. Since nitrous acid (HONO) was not measured during our  
152 observation, it was fixed as 2% of the observed NO<sub>2</sub> concentration. This constant ratio is well  
153 observed in different field studies and performed well in previous box model studies (Tan et  
154 al., 2019). Before each simulation, the model was run 3 days as spin up to reach a steady state  
155 for unmeasured species (e.g., OH and NO<sub>3</sub> radicals).

156 The comparison of simulated and observed O<sub>3</sub> and HCHO concentrations are shown in  
157 Figure S1 and Figure S2. The index of agreement (IOA), mean bias (MB) and normalized mean  
158 bias (NMB) are used to evaluate the model performance. These three parameters can be  
159 calculated by Equation (2) to (4), where S<sub>i</sub>, O<sub>i</sub>, and  $\bar{O}$  are the simulated, observed, and average  
160 observed value of the target compound. In this study, the IOA, MB and NMB of O<sub>3</sub> was 0.90,  
161 0.76 and 10%, respectively. These results suggest that the model can reasonably reproduce the  
162 variations of O<sub>3</sub> and could be used for further analysis. As for HCHO, the IOA, MB, and NMB  
163 was 0.74, 2.43 and 48%, respectively. In general, the model overestimated HCHO  
164 concentration, especially on July 29 and July 30. According to previous studies, the  
165 inconsistency between simulated and observed HCHO is attributed to uncertainties in the  
166 treatment of dry deposition, faster vertical transport, uptake of HCHO and fresh emissions of  
167 VOCs precursors (Li et al., 2014). In addition, primary HCHO sources can contribute up to 76%  
168 of total HCHO concentration in urban areas (Li et al., 2010). However, due to the lack of  
169 primary HCHO sources for areas around DSL, primary HCHO emissions were not included in  
170 our model. Although there exists some bias, the model results still provide valuable information  
171 of secondary formation of HCHO at suburban areas. To assess the reliability of model results  
172 without OH observation, we compared the OBM-simulated OH concentration with that  
173 calculated using the ratio of ethylbenzene (E) and m,p-xylene (X) that share common emission  
174 sources but with different reactivity with OH radicals (shown in Equation (5)~(8)):

$$IOA = 1 - \frac{\sum(S_i - O_i)^2}{\sum(|S_i - \bar{O}| + |O_i - \bar{O}|)^2} \quad (2)$$

$$MB = \frac{\sum(S_i - O_i)}{N} \quad (3)$$

$$NMB = \frac{\sum(S_i - O_i)}{\sum O_i} \times 100\% \quad (4)$$



$$[X]_t = [X]_0 \times e^{-[OH] \times k_{X, OH} \times t} \times f_{d, B} \quad (7)$$

$$[OH]_{\frac{E}{X}} = \frac{1}{t \times (k_{E, OH} - k_{X, OH})} \times \left[ \ln \left( \frac{[E]}{[X]} \right)_0 - \ln \left( \frac{[E]}{[X]} \right)_t \right] \quad (8)$$

175 where  $[X]_0$  and  $[X]_t$  are the mixing ratio of X at the initial time and after transport time t.  $k_{X, OH}$   
 176 is the temperature dependent reaction rate coefficient of m,p-xylene with OH, which was taken  
 177 from the IUPAC database (<http://iupac.pole-ether.fr/>), whereas  $f_{d, B}$  is the dilution factor of m,p-  
 178 xylene in the atmosphere. In this study, we assume that the rates of turbulent mixing and  
 179 horizontal convection are similar for E and X. Therefore, during the transport time  $\Delta t$ , the  
 180 dilution factor of E and X are the same. Therefore, rearranging Equation (7) and extending this  
 181 analysis to E and X will yield Equation (8), where  $[OH]_{E/X}$  is the estimated regional mixing  
 182 ratio of OH by ethylbenzene and m, p-xylene ratio. The calculated average regional  
 183 concentrations of OH ( $8.39 \pm 5.11 \times 10^6$  molecules  $\text{cm}^{-3}$ ) was in the same magnitude of the  
 184 OBM-simulated result ( $4.59 \pm 5.11 \times 10^6$  molecules  $\text{cm}^{-3}$ ), suggesting that the OBM-simulated  
 185 radical concentration is reliable.

186 To quantify the changes of atmospheric oxidative capacity (AOC) in response to isoprene  
 187 chemistry, two parallel scenarios (S0 and S1) were conducted with isoprene chemistry disabled  
 188 in S1. In both cases, identical chemical mechanism and meteorological conditions were used  
 189 to drive the model simulations. A comparative analysis of the scenarios revealed the impact of  
 190 isoprene chemistry on AOC and secondary formation of  $\text{O}_3$  and  $\text{HCHO}$ .

191 **3. Results and discussions**

192 **3.1 Overview of the observations**

193 To investigate the impact of local chemistry on ozone formation and avoid the influence  
194 of emission transportation, five days under stagnant condition (with daily average wind speed  
195 less than 2m/s and maximum daily 8-h average (MDA8) O<sub>3</sub> concentration >75 ppb) were  
196 identified as typical local chemistry cases. Figure 2 shows the time series of observed  
197 meteorological parameters (P, T, and RH), trace gases (NO, NO<sub>2</sub> and O<sub>3</sub>), isoprene and HCHO  
198 on selected days. During those episodes, the air masses reaching the site were mainly from  
199 southeast and southwest (Figure 2). The weak wind was not conducive to the regional  
200 transportation of air pollutants. The observed O<sub>3</sub>, NO<sub>2</sub>, NO, CO, and TVOC ranged from 1.40  
201 to 155.40 ppbv (52.72 ± 44.43 ppbv, average value, the same below), 5.36 to 57.95 ppbv (21.58  
202 ± 12.88 ppbv), 0.75 to 54.51 ppbv (5.40 ± 8.13 ppbv), 400 to 960 ppbv (597 ± 153 ppbv), and  
203 2.34 to 20.33 ppbv (7.28 ± 4.32 ppbv) respectively. During the five episodes, the average  
204 concentration of alkanes (13.97 ± 9.12 ppbv), alkenes (3.27 ± 2.31 ppbv) and aromatics (4.93  
205 ± 2.69 ppbv) was about 53%, 18%, and 50% respectively, higher than that of the whole  
206 observation period. The conditional probability function (CPF) is applied to reveal the  
207 relationship between high O<sub>3</sub> concentrations and wind (Figure 3). The detailed description of  
208 CPF can be found in the supplementary information (Text S1). The results suggest that high  
209 O<sub>3</sub> concentrations (>131 ppb) was usually observed when the site was influenced by weak  
210 south wind. This implies that the high O<sub>3</sub> was mostly formed locally. Although this site is  
211 distant from urban areas, high levels of NO were found during early morning, emanating  
212 particularly from nearby heavy-duty vehicle emissions. As for NO<sub>2</sub>, only one peak was found  
213 at dusk. This was in contrast with previous results in urban areas (Zhang et al., 2019). It is  
214 worth noting that NO<sub>2</sub> and O<sub>3</sub> concentrations were high even during nighttime, suggesting that  
215 the AOC remained high at nighttime. It should also be noted that, flat CO pattern was found

216 during morning when NO<sub>x</sub> peaks were observed. This inconformity can be attributed to the  
217 coarse resolution of CO analyzer (about 80 ppbv) and CO emission source (mainly gasoline  
218 vehicles in terms of vehicle exhaust) while NO<sub>x</sub> is mainly emitted by heavy-duty vehicle  
219 exhausts. Therefore, since DSL site is far from urban area, it is unlikely to have gasoline  
220 vehicles in early morning. On the contrary, there are sometimes heavy-duty trucks passing by,  
221 causing peaks of NO in early morning.

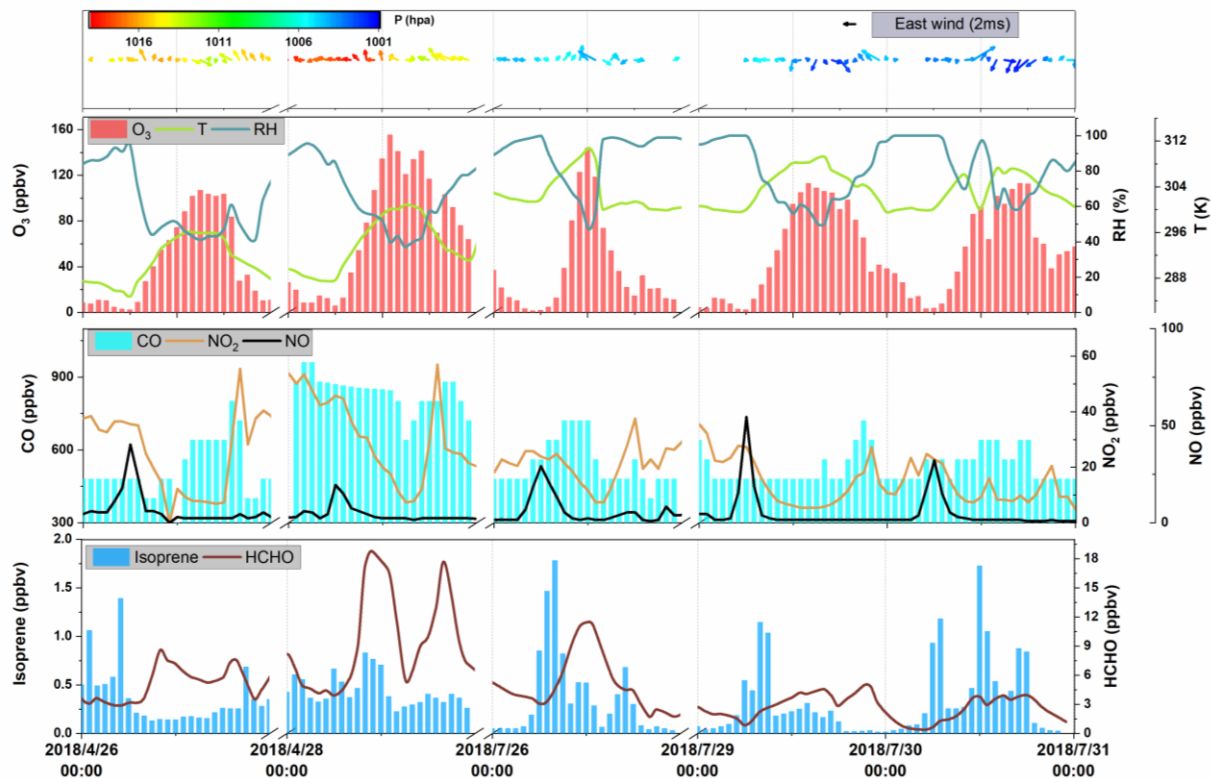
222 The daily average isoprene concentration was  $0.37 \pm 0.36$  ppbv, and is comparable to the  
223 observations by Gong et al. (2018) at a forested mountaintop site ( $0.287 \pm 0.032$  ppbv). To  
224 estimate the influence of isoprene on atmospheric oxidation capability, we adopted the  
225 approach by Zhu et al. (2020) to calculate the OH reactivity ( $k_{OH}$ ). Results suggested that  
226 isoprene, accounting for ~19% of the total  $k_{OH}$ , was the most significant VOC species with  
227 respect to  $k_{OH}$  ( $0.89 \pm 0.44$  s<sup>-1</sup>). This indicates the significant role of isoprene in the  
228 photochemistry of a suburban area. The average HCHO was  $5.01 \pm 3.80$  ppbv, which was ~2  
229 times of that observed at a rural site of Hong Kong (Yang et al., 2020). It is worth noting that  
230 HCHO could reach an average of 18.69 ppbv at midday.

231 Based on explicit calculation, the total concentration of OVOC was obtained. However,  
232 due to the complexity of OVOC formation, which could have hundreds of precursors for just  
233 one OVOC specie and the complex chain reactions converting VOCs to OVOCs, it is difficult  
234 to derive an accurate relationship between VOCs and OVOCs. But since VOCs were mainly  
235 oxidized by OH and O<sub>3</sub> during daytime, in this study, we chose multi-linear regression model  
236 (Eq.(9) ) to roughly explore the relationship between VOCs and simulated OVOCs.

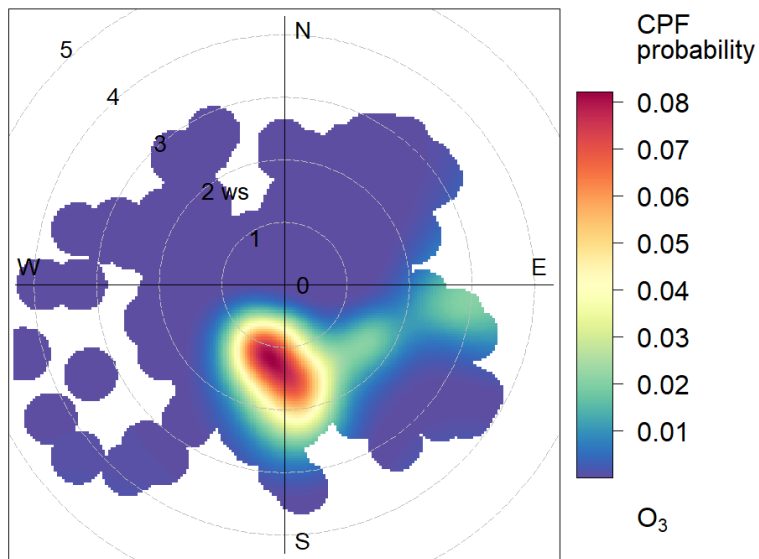
$$[OVOC] = \beta_0 + \beta_1[Alkane] + \beta_2[Alkene] + \beta_3[Aromatic] + \beta_4[OH] + \beta_5[O_3] \quad (9)$$

237 where  $\beta_0$ ,  $\beta_1$ ,  $\beta_2$ ,  $\beta_3$ ,  $\beta_4$ , and  $\beta_5$  are the coefficients from linear regression; [OVOC] and [OH]  
238 are the predicted concentration of OVOC and OH, respectively; [Alkane], [Alkene],  
239 [Aromatic], [O<sub>3</sub>] are the observed concentration of alkanes, alkenes, aromatics, and O<sub>3</sub>,

240 respectively. The Sig value and statistical reliability criteria (R) was 0.000 and 0.853 (shown  
 241 in Table S2 and Figure S3), respectively, indicating that the linear relationship represented by  
 242 equations (9) is statistically reliable. Similarly, the  $\beta_1$ ,  $\beta_2$ ,  $\beta_3$  was 0.027, 0.623, and 0.820,  
 243 respectively, suggesting that alkenes and aromatics are significant for the simulated OVOC  
 244 concentration.



245  
 246 **Figure 2. Time series of hourly averages for O<sub>3</sub>, CO, NO, NO<sub>2</sub>, isoprene, HCHO, and meteorological**  
 247 **parameters.**



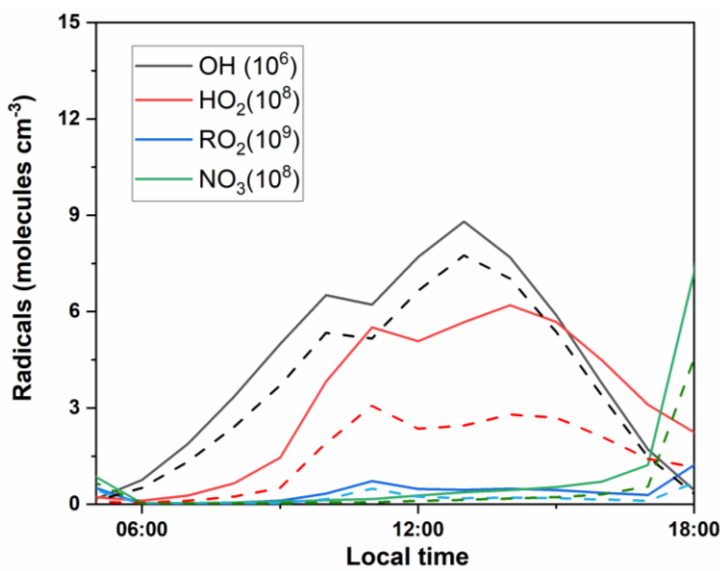
248 **CPF at the 95th percentile (=131)**

249 **Figure 3. CPF polar plot of O<sub>3</sub> at DSL station.**

250 **3.2 Simulated concentrations of radicals**

251 Figure 4 shows the simulated average daytime variation of major radicals in the base  
 252 scenario (S0). It should be noted that, the discussion below is limited to local conditions (cases  
 253 with average wind speed lower than 2m/s), since transportation of emissions are not considered  
 254 in the 0-dimensional model. The daily average simulated concentration of OH, HO<sub>2</sub>, RO<sub>2</sub>, and  
 255 NO<sub>3</sub> was  $4.88 \times 10^6$ ,  $3.49 \times 10^8$ ,  $0.31 \times 10^9$ , and  $0.31 \times 10^8$  molecules cm<sup>-3</sup>, respectively. The  
 256 simulated daily average OH concentration is comparable to a summertime simulation in  
 257 Beijing ( $9 \times 10^6$  molecules cm<sup>-3</sup>) (Liu et al., 2019) and at a suburban site in Hong Kong in 2013  
 258 ( $1.5 \pm 0.2 \times 10^6$  molecules cm<sup>-3</sup>) (Xue et al., 2016). In addition, the average simulated daytime  
 259 OH concentration was ~33% lower than that simulated at a forested mountaintop site in  
 260 southern China (Gong et al., 2018). To verify the performance of OBM model, regional  
 261 daytime mixing ratios of OH were also calculated by a parameterization method using  
 262 measured ethylbenzene and *m,p*-xylene ratios. The calculated average regional concentrations  
 263 of OH ( $8.39 \pm 5.11 \times 10^6$  molecules cm<sup>-3</sup>) was in the same magnitude of the OBM-simulated

264 result ( $4.88 \pm 5.11 \times 10^6$  molecules  $\text{cm}^{-3}$ ), suggesting that the OBM-simulated radical  
 265 concentration is reliable. Furthermore, at the DSL site, the simulated maximum  $\text{HO}_2$   
 266 concentration ( $6.19 \times 10^8$  molecules  $\text{cm}^{-3}$ ) was close to that reported in Beijing ( $6.8 \times 10^8$   
 267 molecules  $\text{cm}^{-3}$ ) (Liu et al., 2012), but was  $\sim 32\%$  higher than that in Wuhan ( $4.7 \times 10^8$  molecules  
 268  $\text{cm}^{-3}$ ) (Zhu et al., 2020a). Due to high reactivity of  $\text{RO}_2$  and high concentration of  $\text{HO}_x$ ,  $\text{RO}_2$   
 269 kept low level during daytime. As for  $\text{NO}_3$ , it can be quickly decomposed during daytime,  
 270 leading to the negligible concentration in the daytime.



271  
 272 **Figure 4. Simulated average daytime variation of OH,  $\text{HO}_2$ ,  $\text{RO}_2$  and  $\text{NO}_3$  in S0 (solid lines) and S1 (dash  
 273 lines).**

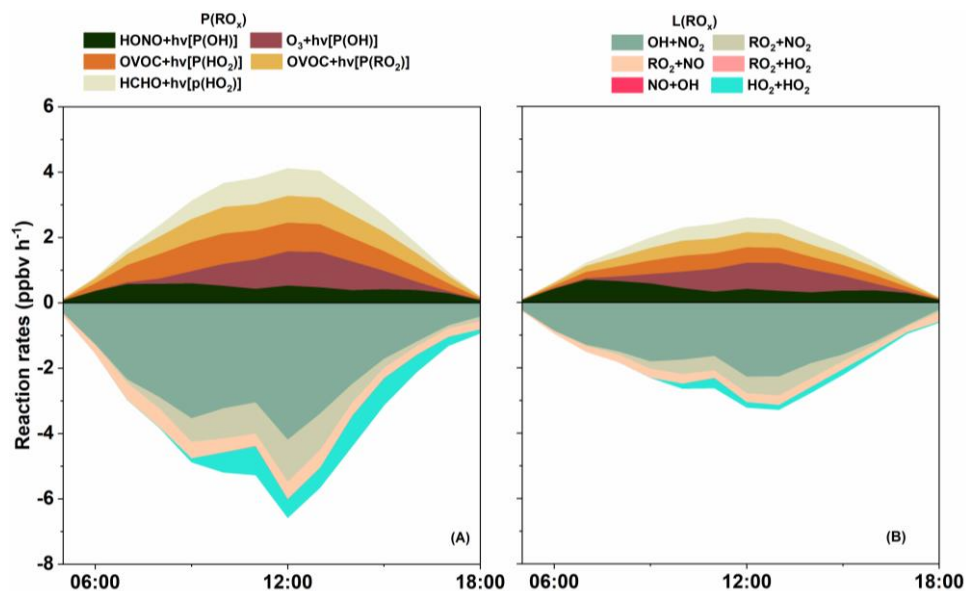
### 274 3.3 Recycling of ROx radicals

275 Figure 5(A) shows the primary sources of ROx in S0 and its detailed daytime budget.  
 276 Minor ROx sources, e.g. ozonolysis of alkenes, are not shown in the figure. Photolysis of  $\text{O}_3$   
 277 was the predominant primary source of OH, with a daytime mean production rate of 0.50 ppbv  
 278  $\text{h}^{-1}$ , which was comparable to that found by Liu et al. (2012) in Beijing, but was 0.40 ppbv  $\text{h}^{-1}$   
 279 lower than the result reported by Xue et al. (2016). Similarly, another important OH source is  
 280 the photolysis of  $\text{HONO}$ , contributing 0.32 ppbv  $\text{h}^{-1}$  of daytime OH production in our  
 281 simulation. This result is much lower than other related studies (Liu et al. (2019) and Xue et al.

282 (2016)), possibly due to the excessive constrain on HONO (since HONO was not directly  
283 monitored) during our experiment.

284 Sensitivity analysis was conducted to quantify the influence of different HONO/NO<sub>2</sub> ratio  
285 on radical recycling (Text S2, Figure S4 and Table S1). As expected, a lower HONO/NO<sub>2</sub> ratio  
286 leads to a lower HONO concentration, and subsequently less OH generation from the  
287 photolysis of HONO. The sensitivity analysis shows that when HONO/NO<sub>2</sub> ratio is 0.005, the  
288 daytime OH level could decrease by 15.28%. Conversely, a higher HONO/NO<sub>2</sub> (e.g., 0.04) can  
289 promote OH concentration by 14.08%. This result illustrates the importance of HONO  
290 photolysis in the generation of OH, and therefore simultaneous ambient measurements of  
291 HONO is highly recommended for future analysis of local radical recycling. Regarding HO<sub>2</sub>,  
292 the photolysis of OVOC (excluding HCHO) is the predominant source with a daytime mean  
293 production rate of 0.65 ppbv h<sup>-1</sup> and maxima of 0.92 ppbv h<sup>-1</sup>, which is comparable to Xue et  
294 al. (2016). The photolysis of HCHO can also contribute 0.48 ppbv h<sup>-1</sup> to the daytime production  
295 of HO<sub>2</sub>, which is close to the results of Xue et al. (2016). As for RO<sub>2</sub>, the photolysis of OVOC  
296 was the largest source (0.57 ppbv h<sup>-1</sup>), which was relatively lower than the results found at an  
297 urban site (Liu et al., 2012). Therefore, regarding RO<sub>x</sub> in DSL site, the daytime primary radical  
298 production was dominated by the photolysis of OVOC (except for HCHO), followed by the  
299 photolysis of HCHO and O<sub>3</sub>. However, the photolysis of HONO can become the overwhelming  
300 RO<sub>x</sub> source around sunrise, which suggests that HONO can be an important OH reservoir  
301 species at night. Summing up all the sources of RO<sub>x</sub> gives a total primary daytime RO<sub>x</sub>  
302 production rate of 2.55 ppbv h<sup>-1</sup> (0.84 ppbv h<sup>-1</sup> for OH, 1.14 ppbv h<sup>-1</sup> for HO<sub>2</sub>, and 0.57 ppbv  
303 h<sup>-1</sup> for RO<sub>2</sub>), which was 61~69% lower than those in Beijing (6.6 ppbv h<sup>-1</sup>, Liu et al. (2012))  
304 and Hong Kong (8.11 ppbv h<sup>-1</sup>, Xue et al. (2016)), indicating that the recycling of RO<sub>x</sub> in  
305 Beijing and Hong Kong could be much reactive.

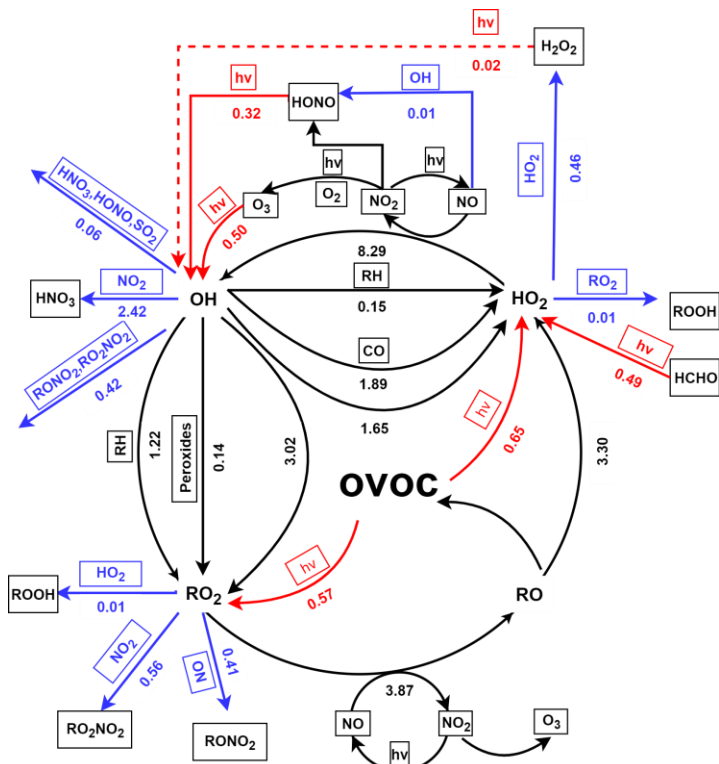
306 RO<sub>x</sub> radicals are ultimately removed from the atmosphere via deposition of radical  
 307 reservoir species, e.g. H<sub>2</sub>O<sub>2</sub>, HNO<sub>3</sub>, and ROOH (Liu et al., 2012). The terminate processes of  
 308 RO<sub>x</sub> was dominated by their reactions with NO<sub>x</sub>. Specifically in this study, the reaction of  
 309 OH+NO<sub>2</sub>, RO<sub>2</sub>+NO<sub>2</sub>, RO<sub>2</sub>+NO, forming HNO<sub>3</sub>, RO<sub>2</sub>NO<sub>2</sub>, and RONO<sub>2</sub>, accounted for 2.42,  
 310 0.56, and 0.41 ppbv h<sup>-1</sup> of the daytime RO<sub>x</sub> radical sink, respectively. This is consistent with  
 311 the understanding that reactions with NO<sub>x</sub> usually dominate the radical sink under high NO<sub>x</sub>  
 312 environments (Xue et al., 2016; Liu et al., 2012). In addition, RONO<sub>2</sub> and RO<sub>2</sub>NO<sub>2</sub> could in  
 313 turn react with OH, leading to 0.41 ppbv h<sup>-1</sup> of daytime OH sinks (Figure 6). Summing up the  
 314 primary sources and sinks gives a negative value of net RO<sub>x</sub> production, suggesting that the  
 315 RO<sub>x</sub> was in a stage of gradual depletion.



316  
 317 **Figure 5. Simulated primary daytime sources and sink of RO<sub>x</sub> in S0 (A) and S1 (B).**

318 Furthermore, the daytime (6:00-18:00) average budget of RO<sub>x</sub> is shown in Figure 6.  
 319 Evidently, the production of OH was dominated by the reaction of HO<sub>2</sub>+NO (8.29 ppbv h<sup>-1</sup>)  
 320 in RO<sub>x</sub> recycling, whereas RO<sub>2</sub> was produced by the reaction of OH with OVOC (3.02 ppbv  
 321 h<sup>-1</sup>), alkyl (RH) (1.21 ppbv h<sup>-1</sup>), and peroxides (0.14 ppbv h<sup>-1</sup>). Besides, the reaction of  
 322 RO<sub>2</sub>+NO can result in strong production of RO (3.87 ppbv h<sup>-1</sup>). Moreover, the reaction of RO  
 323 and O<sub>2</sub> was the major contributor to HO<sub>2</sub> production, followed by the reaction of OH with CO

324 (1.89 ppbv h<sup>-1</sup>), OVOC (1.59 ppbv h<sup>-1</sup>), and RH (0.15 ppbv h<sup>-1</sup>). It is worth noting that the top  
325 two fast reactions within the recycling of RO<sub>x</sub> (HO<sub>2</sub>+NO and RO<sub>2</sub>+NO) were related to NO<sub>x</sub>.  
326 As mentioned in the study of Liu et al. (2012), this result could be mainly due to the abundance  
327 of NO (e.g. ~50 ppbv in the morning). Obviously, these recycling processes dominate the total  
328 production of OH, HO<sub>2</sub> and RO<sub>2</sub> radicals. As suggested in the study of Xue et al. (2016) and  
329 Liu et al. (2012), the radical propagation is efficient and enhances the effect of the newly  
330 produced radicals in the polluted atmospheres with the co-existence of abundant NO<sub>x</sub> and  
331 VOCs.



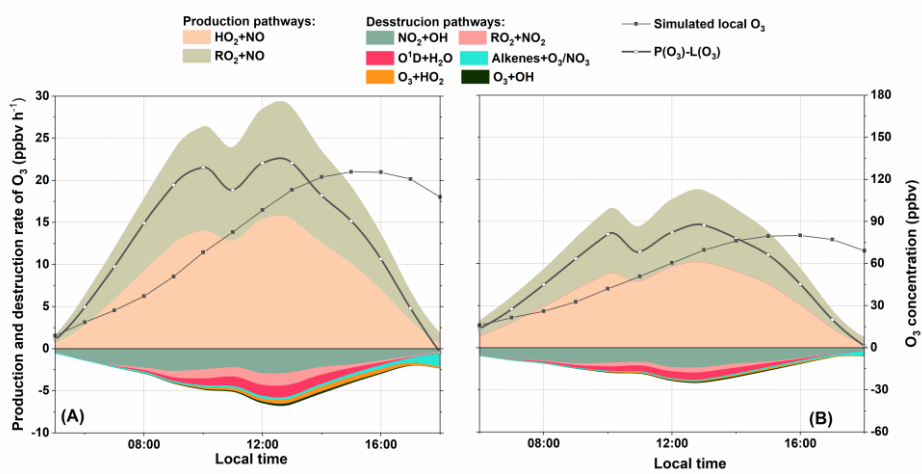
332  
333 **Figure 6. Summary of daytime (06:00-18:00) average budgets of ROx radicals (in ppbv h<sup>-1</sup>). Primary ROx**  
334 **sources and sinks are in red and blue, respectively, and the black lines represent the processes in ROx**  
335 **and NOx recycling.**

336 3.4 Formation and sink of O<sub>3</sub>

337 Figure 7 illustrates the diurnal variation of simulated O<sub>3</sub> concentration, net production rate  
338 (including the formation and sink pathways) in S0. In the troposphere, O<sub>3</sub> is formed via the  
339 reactions of NO with peroxy radicals (e.g. HO<sub>2</sub> and RO<sub>2</sub>) (Liu et al., 2012; Xue et al., 2016;

340 Zhu et al., 2020a). Consequently, the daytime reaction of  $\text{HO}_2+\text{NO}$  and  $\text{RO}_2+\text{NO}$  contributed  
 341 an average of 9.34 and 8.52 ppbv  $\text{h}^{-1}$  of the  $\text{O}_3$  produced. Coincidentally, the maximum rate of  
 342  $\text{HO}_2+\text{NO}$  (15.36 ppbv  $\text{h}^{-1}$ ) and  $\text{RO}_2+\text{NO}$  (13.26 ppbv  $\text{h}^{-1}$ ) both occurred at 13:00 LST. Our  
 343 results reveal a total daytime production rate of  $\text{O}_3$  ( $\text{P}(\text{O}_3)$ ): the sum of  $\text{HO}_2+\text{NO}$  and  $\text{RO}_2+\text{NO}$   
 344 at 17.86 ppbv  $\text{h}^{-1}$ , which is in line with related study in Beijing (32 ppbv  $\text{h}^{-1}$ , Liu et al. (2012))  
 345 and Hong Kong (6.7 ppbv  $\text{h}^{-1}$ , Liu et al. (2019)).

346 Due to the fast cycling of both  $\text{O}_3$  and  $\text{NO}_2$ , the sink of  $\text{O}_3$  resulted from several reactions  
 347 leading to the destruction of  $\text{O}_3$  and  $\text{NO}_2$ . In our case, the reaction of  $\text{NO}_2+\text{OH}$  is the  
 348 predominant scavenging pathway of  $\text{O}_3$ , with an average daytime reaction rate of 1.89 ppbv  $\text{h}^{-1}$   
 349 (49%, percentage of the total  $\text{O}_3$  sink rate.). This is comparable to the study of Liu et al. (2012  
 350 and 2019). In addition, the reaction of  $\text{RO}_2+\text{NO}_2$  was the second contributor to  $\text{O}_3$  sink with a  
 351 mean contribution of 0.62 ppbv  $\text{h}^{-1}$  (16%). Other pathways, e.g. photolysis of  $\text{O}_3$ , ozonolysis  
 352 of alkenes, and  $\text{O}_3+\text{HO}_2$ , altogether contributed 1.11 ppbv  $\text{h}^{-1}$  of the total daytime  $\text{O}_3$  sink rate.  
 353 Also, the daytime mean  $\text{L}(\text{O}_3)$  was 3.87 ppbv  $\text{h}^{-1}$ , which was  $\sim 22\%$  of  $\text{P}(\text{O}_3)$ , suggesting that  
 354  $\text{O}_3$  could efficiently accumulate during daytime. The net production of  $\text{O}_3$  ( $\text{P}(\text{O}_3)-\text{L}(\text{O}_3)$ ) is also  
 355 shown in Figure 7. Our results reveal a maximum  $\text{O}_3$  concentration at around 16:00 LST, which  
 356 was also observed in other suburban sites (Zong et al., 2018; Zhang et al., 2019).



357  
 358 **Figure 7. Simulated average diurnal profiles of  $\text{O}_3$  formation and sink rates (ppbv  $\text{h}^{-1}$ ) in S0 (A) and S1  
 359 (B).**

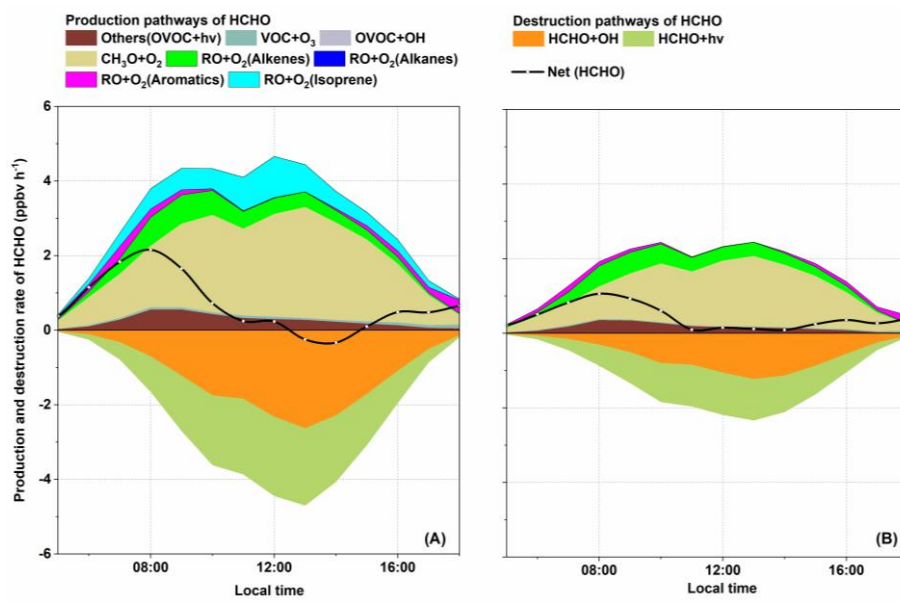
360 **3.5 Formation and sink of HCHO**

361 As aforementioned, high levels of HCHO was observed at DSL. Figure 8 (A) shows the  
362 production and sink pathways of HCHO in S0. In this study, the local HCHO formation was  
363 dominated by the reaction of RO+O<sub>2</sub>, accounting for ~90% of the total production rate. Further  
364 classification of RO+O<sub>2</sub> pathway suggested that the oxidation of CH<sub>3</sub>O made a significant  
365 contribution of ~47%, followed by RO (from isoprene) + O<sub>2</sub> reaction (12%) and RO (from  
366 aromatics) + O<sub>2</sub> reaction (~11%). This result is comparable to the study of Yang et al. (2020;  
367 2018). During the day, isoprene is the most important VOC species in the production of HCHO  
368 with a mean rate of 0.48 ppbv h<sup>-1</sup>. As stated earlier, the study site is surrounded by dense  
369 vegetation, which provides abundant biogenic isoprene. As a result, over 90% of the daytime  
370 isoprene was oxidized by OH radicals (Figure S5). Based on the MCMv3.3.1, several RO<sub>2</sub>  
371 species (e.g. ISOP34O<sub>2</sub>, ISOPDO<sub>2</sub>, ISOPCO<sub>2</sub>, CISOPAO<sub>2</sub>, ISOPAO<sub>2</sub>) can be generated  
372 during the OH-initiated degradation process of isoprene (Jenkin et al., 2015). For instance, with  
373 the presence of NO, isoprene-originated RO<sub>2</sub> can transfer into RO (e.g. ISOPDO, ISOP34O,  
374 ISOPAO). The subsequent degradation processes of isoprene-related RO, especially ISOP34O,  
375 ISOPDO, ISOPAO and ISOPBO, are closely related to the formation of HCHO (Jenkin et al.,  
376 2015). In other sources of HCHO, such as the reaction between VOC and O<sub>3</sub>, photolysis of  
377 OVOC and the reaction of OVOC+OH only contributed small amount of the total production  
378 rate during whole day.

379 In this study, it is noteworthy that the two dominant pathways for HCHO depletion were  
380 the photolysis of HCHO (~52%) and the reaction of HCHO+OH (~48%). On the other hand,  
381 the net HCHO production rate (equals to P(HCHO) + L(HCHO)) as shown in Figure 8. It is  
382 evident that after sunrise, the net production rate of HCHO rose gradually to a peak of ~1.6  
383 ppbv h<sup>-1</sup> at 8:00 (similar to the results by Yang et al. (2018)). Thereafter, at around 12:00 LST,  
384 net(HCHO) dropped to ~0 ppbv h<sup>-1</sup>, which was roughly consistent with our observation,

385 showing the HCHO peak occurs at around 12:00. In addition, a negative net(HCHO) was  
 386 exhibited between 13:00 and 14:00, . Although the reaction of RO+O<sub>2</sub> quickly produced HCHO  
 387 in the afternoon, the depletion pathways, especially the photolysis of HCHO, became more  
 388 competitive, leading to the net reduction of HCHO. This also indicates that strong  
 389 photochemical reactions do not monotonously profit the accumulation of HCHO, it can also  
 390 constrain high HCHO levels in certain situations. After 14:00, the photolysis of HCHO dropped  
 391 rapidly and the net depletion of HCHO back to ~0 ppbv h<sup>-1</sup> at around 15:00. The daytime net  
 392 HCHO production rate was 0.70 ppbv h<sup>-1</sup>, which was comparable to result of Yang et al. (2018).

393 The above analysis indicates that the photolysis of OVOC, HCHO, O<sub>3</sub> and HONO was  
 394 the primary source of ROx, which offers high oxidizing environment for the degradation of  
 395 VOCs. As a typical by-product in the degradation of several VOCs, HCHO can be quickly  
 396 formatted during the day. The insight into the detailed photochemical processes shows the  
 397 important role of isoprene in the formation of HCHO.



398

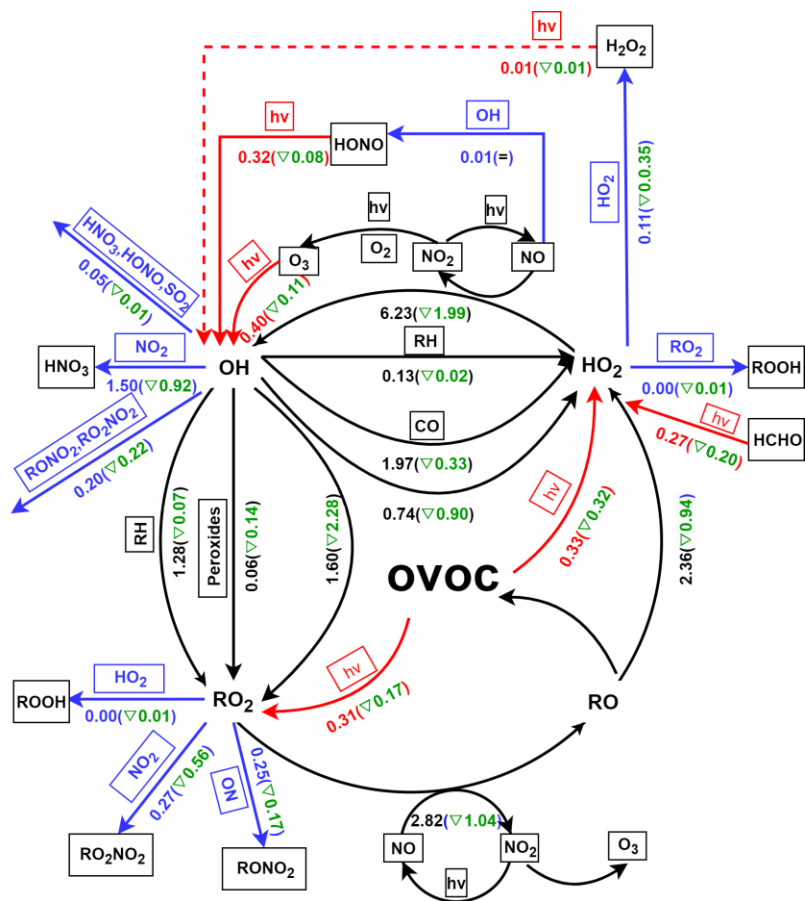
399 **Figure 8. Simulated average daytime profiles of net rate (net (HCHO)), breakdown HCHO production  
 400 rate and sink rate (ppbv h<sup>-1</sup>) in S0 (A) and S1 (B).**

401 **3.6 Impacts of isoprene chemistry on photochemistry**

402 **3.6.1 Impact on RO<sub>x</sub> budget**

403 To compare the importance of isoprene and other abundant VOCs in local chemistry at  
404 DSL site, sensitivity analysis was conducted for the modelled O<sub>3</sub>, HCHO, and OH  
405 concentrations without the input of active VOCs (toluene, ethylene, ethylbenzene, ethane,  
406 acetylene, xylene, propene, and isoprene). Results suggested that, although the average  
407 isoprene concentration was only 0.37 ± 0.36 ppbv, cutting isoprene input can lead to obvious  
408 drop in simulated O<sub>3</sub>, HCHO, and OH, which was comparable to that of cutting EXT and  
409 alkenes, indicating the significant role of isoprene in local photochemical processes (Figure  
410 S6). In addition, the degradation of isoprene is closely linked to the cycling of RO<sub>x</sub>. To roughly  
411 explain the impact of isoprene chemistry on RO<sub>x</sub> budget, we carried out a parallel simulation  
412 (S1) where isoprene chemistry is disabled (Figure 9). The diurnal variation of OH, HO<sub>2</sub>, RO<sub>2</sub>  
413 and NO<sub>3</sub> in S1 is also shown in Figure 4 (B) which clearly suggests the decline in RO<sub>x</sub> and  
414 NO<sub>3</sub> without isoprene input. To investigate the underlying causes, we calculated the production  
415 rate of RO<sub>x</sub> (P(RO<sub>x</sub>)) and loss rate of RO<sub>x</sub> (L(RO<sub>x</sub>)) in S1, respectively (Figure 5 (B)).  
416 Comparative analysis revealed a decreasing trend for most of the reaction rates in P(RO<sub>x</sub>) and  
417 L(RO<sub>x</sub>) in S1. This strongly indicates that the absence of isoprene slows down the RO<sub>x</sub>  
418 recycling. Generally, considering that the photolysis of OVOC (0.67 ppbv h<sup>-1</sup>) was still the  
419 predominant primary source of RO<sub>x</sub>, but without isoprene, the photolysis rate of OVOC  
420 decreased by 0.49 ppbv h<sup>-1</sup>. Moreover, the total production and depletion rate of OH dropped  
421 to 6.96 and 7.51 ppbv h<sup>-1</sup>, respectively. Although the absence of isoprene could reduce the  
422 consumption of OH, the OH concentration would be reduced by ~16% compared to S0,  
423 suggesting that the amount of OH produced via isoprene chemistry is large enough to  
424 compensate for the shift from OH to peroxy radicals in the RO<sub>x</sub> family. As for RO<sub>2</sub>, the daytime  
425 production and sink rate falls to 3.25 and 3.34 ppbv h<sup>-1</sup>, respectively. This means the

426 concentration of RO<sub>2</sub> would be in a stage of gradual decrease. In addition, the absence of  
427 isoprene could also reduce RO<sub>2</sub> concentration by ~20%, suggesting that isoprene was an  
428 important source of RO<sub>2</sub> at DSL site. As for HO<sub>2</sub>, drastic decrease of ~53% was found in S1.  
429 The above-mentioned decrease in RO<sub>x</sub> obviously could not be explained solely by the removal  
430 of isoprene-related radicals. Sensitivity assessment of the model results shows that OVOC  
431 concentrations decreased drastically (~41%) after cutting isoprene (e.g. ~37% decrease in  
432 formaldehyde, ~65% decrease in methylglyoxal, ~51% decrease in glyoxal, ~100% decrease  
433 in methacrolein (MACR), and ~100% decrease in methyl vinyl ketone (MVK)). The decrease  
434 in OVOC can further pull-down substantial amount of primary RO<sub>2</sub> and HO<sub>2</sub> (Figure 6 and  
435 Figure 9). It is interesting to note that, taking away isoprene also causes a drop of NO<sub>3</sub> (~23%).  
436 This result can be attributed to the decrease of secondary production of O<sub>3</sub> (~35%), which can  
437 further reduce the formation of NO<sub>3</sub> especially at night.



439 **Figure 9. Summary of daytime (06:00-18:00) average budgets of ROx radicals (in ppbv h<sup>-1</sup>) in S1.**  
440 Primary ROx sources and sinks are in red and blue, respectively, and the black lines represent the  
441 processes in ROx and NOx recycling. Values in the brackets represent the difference between S1 and S0.

#### 442 **3.6.2 Impact on O<sub>3</sub> formation**

443 To investigate the detailed impact of isoprene on O<sub>3</sub> formation, the production and sink  
444 pathways of O<sub>3</sub> in S1 was also quantified (see Figure 7 (B)). Notably, the simulated maximum  
445 and daily average O<sub>3</sub> dropped to 84.95 and 41.23 ppbv, respectively, which is ~35% and ~34%  
446 lower than that in S0. By comparing S1 and S0, the absence of isoprene can reduce all the  
447 production and sink pathways of O<sub>3</sub>. For example, the rate of the two major production  
448 pathways of O<sub>3</sub> (HO<sub>2</sub>+NO and RO<sub>2</sub>+NO) decreased by ~37% and ~45%, respectively. This can  
449 be attributed to the drop in the concentration of HO<sub>2</sub> and RO<sub>2</sub> radical in S1. Similarly, the  
450 absence of isoprene in O<sub>3</sub> depletion caused a decrease of 0.31 ppbv h<sup>-1</sup> in the reaction rate of  
451 alkene+O<sub>3</sub>/NO<sub>3</sub>, followed by RO<sub>2</sub>+NO<sub>2</sub> (0.22 ppbv h<sup>-1</sup>) and NO<sub>2</sub>+OH (0.265 ppbv h<sup>-1</sup>).  
452 Apparently, the absence of isoprene will reduce the total concentrations of alkenes and can  
453 further lead to the decrease of RO<sub>2</sub> and OH level, which ultimately slows down the depletion  
454 pathways of O<sub>3</sub>. Eventually, the absence of isoprene caused a decrease of 5.78 ppbv h<sup>-1</sup> in the  
455 daytime mean net production rate of O<sub>3</sub>. Hence, isoprene chemistry plays an important role in  
456 the local O<sub>3</sub> formation at DSL site.

#### 457 **3.6.3 Impact on HCHO formation**

458 The analysis of S0 revealed the important role of isoprene, aromatics, and alkenes in the  
459 production of HCHO. To investigate the chain effect of isoprene chemistry on HCHO  
460 production, the major reactions that dominate the formation and depletion of HCHO in S1 were  
461 also analyzed by OBM model (Figure 8 (B)). Comparisons between S0 and S1 shows that the  
462 daily average HCHO decreased by 2.90 ppbv (~39%) when isoprene chemistry is cut off.  
463 Obviously, the drop in HCHO concentration cannot be solely illustrated by the absence of RO  
464 (from isoprene). As aforementioned, the absence of isoprene slows down the recycling of ROx

465 and can further lead to decrease in RO<sub>x</sub> concentration. Based on the OBM analysis, the  
466 concentration of CH<sub>3</sub>O, RO (from aromatics), RO (from alkanes), and RO (from alkenes)  
467 decreased by 2.70×10<sup>2</sup> molecule cm<sup>-3</sup>, 1.59×10<sup>5</sup> molecule cm<sup>-3</sup>, 3.35×10<sup>1</sup> molecule cm<sup>-3</sup>, and  
468 3.44 molecule cm<sup>-3</sup>, respectively. The drop in the HCHO precursor concentrations ultimately  
469 led to decrease in the daytime reaction rate of CH<sub>3</sub>O + O<sub>2</sub>, RO (from alkenes) + O<sub>2</sub>, and RO  
470 (from aromatics) + O<sub>2</sub> by 0.66 ppbv h<sup>-1</sup> (~36%), 0.06 ppbv h<sup>-1</sup> (~16%), and 0.06 ppbv h<sup>-1</sup>  
471 (~40%), respectively. The total daytime formation rate of HCHO dropped to 1.71 ppbv h<sup>-1</sup> from  
472 1.66 ppbv h<sup>-1</sup> (~49%) lower than that in S0. As a result of the lower HCHO and OH  
473 concentration in S1, the daily mean depletion rate of HCHO decreased by 1.25 ppbv h<sup>-1</sup> (~49%).  
474 Ultimately, the absence of isoprene pulled down the daily average HCHO level by 1.61 ppbv  
475 (~36%).

476 **3.7 Uncertainty analysis**

477 Due to limitations in the observations, several issues should be noted in the application of  
478 the OBM model to evaluate the local chemistry in the present study. Firstly, methane  
479 concentration, which was set to 1850 ppbv based on previous observations, could be an  
480 overestimation or underestimation. Thus, we conducted sensitivity analysis of modelled O<sub>3</sub>,  
481 OH, and HCHO with different methane values (from 1600 ppbv to 1900 ppbv) (Figure. S7).  
482 The model predicted O<sub>3</sub>, HCHO, and OH concentration with negligible change under different  
483 CH<sub>4</sub> values. Secondly, the photolysis rates directly influence the key photochemical processes  
484 during the day. Since the photolysis rates were not measured during the sampling period, we  
485 also conducted sensitivity analysis by increasing or decreasing the photolysis rates by 20% and  
486 40%. Results showed that the O<sub>3</sub>, HCHO and OH concentration could increase by 51.14%,  
487 34.52%, and 50.38%, respectively, when photolysis rates were increased by 40% (Figure S8).  
488 On the contrary, when photolysis rates were decreased by 40%, O<sub>3</sub>, HCHO and OH  
489 concentration decreased by 50.59%, 30.84%, and 47.24%, respectively (Figure. S6). According

490 to the study by Xu et al. (2013),  $\text{NO}_2$  concentration measured by the molybdenum oxide  
491 converter technique can be significantly overestimated in areas far away from fresh  $\text{NO}_x$   
492 emission sources. Therefore, OBM simulations with reduced  $\text{NO}_2$  concentrations were  
493 conducted. The results suggest that decreasing  $\text{NO}_2$  could increase or decrease of  $\text{O}_3$ ,  $\text{HCHO}$   
494 and  $\text{OH}$  concentrations under different scenarios (Figure S9). Overall, decreasing  $\text{NO}_2$  by 40%  
495 could cause 6.94%, 12.07%, and 6.29% increase in  $\text{O}_3$ ,  $\text{HCHO}$ , and  $\text{OH}$  concentrations,  
496 respectively. Finally, the total surface area of aerosols was obtained from the study of Wang et  
497 al. (2014) and the uncertainty of this value could directly influence the heterogeneous reactions  
498 in this model. Therefore, we conducted sensitive analysis by using increasing or decreasing SA  
499 value by 40% (Figure S10). The results show that  $\text{O}_3$ ,  $\text{HCHO}$ , and  $\text{OH}$  concentrations did not  
500 exhibit obvious changes when SA changed. Hence, accurate measurement data of photolysis  
501 rate and  $\text{NO}_2$  concentration is strongly recommended in further OBM analyses.

## 502 **4. Conclusions**

503 Our observations at a suburban site of the YRD region from April to June in 2018 captured  
504 5 typical local  $\text{O}_3$  formation episodes. The detailed atmospheric photochemistry during these  
505 episodes were analyzed by a typical 0-D box model on a local scale. Under stagnant conditions,  
506 the photolysis of OVOC served as the predominant primary RO<sub>x</sub> sources. RO<sub>x</sub> achieves  
507 efficient recycling with the participation of NO<sub>x</sub>. Influenced by the fast RO<sub>x</sub> recycling, local  
508  $\text{O}_3$  was efficiently produced and accumulated under stagnant conditions. The reactions of RO  
509 radicals with  $\text{O}_2$  dominate the photochemical formation of  $\text{HCHO}$ . The higher atmospheric  
510 oxidative capacity lead to fast degradation of VOCs, which can further lead to high levels of  
511  $\text{HCHO}$  at the DSL site. Specifically, the degradation of RO radicals (e.g. ISOP34O, ISOPDO,  
512 ISOPAO and ISOPBO) from isoprene oxidation play an important role in the photochemical  
513 production of  $\text{HCHO}$ . To investigate the role of isoprene in RO<sub>x</sub> recycle and the formation of  
514 secondary pollutant, a sensitivity scenario without isoprene (S1) input was simulated by OBM

515 model. By comparing S1 to the standard simulation (S0), we find that isoprene chemistry is  
516 important in local RO<sub>x</sub> recycling. The absence of isoprene can obviously decrease the  
517 concentrations of OVOC and the reaction rates in RO<sub>x</sub> propagations, and further reduce the  
518 concentrations of radicals (e.g. OH, HO<sub>2</sub>, RO<sub>2</sub>). Our results indicate that isoprene chemistry  
519 can strongly influence the formation of O<sub>3</sub> and HCHO in the presence of NO<sub>x</sub>. Therefore,  
520 removing isoprene can slow down the reaction of HO<sub>2</sub>+NO and RO<sub>2</sub>+NO by ~37% and ~45%,  
521 respectively, and eventually cause ~34% decrease of O<sub>3</sub>. As a result of the lower O<sub>3</sub>  
522 concentration, average concentration of NO<sub>3</sub> dropped by 23% in S1. The absence of isoprene  
523 can also lead to the decrease of RO (from isoprene) and RO<sub>x</sub> concentration and cause an  
524 obvious drop of HCHO formation (~49%). Furthermore, other biogenic VOCs (BVOCs, such  
525 as terpene and sesquiterpene) can also affect local chemistry via photochemical processes, but  
526 those BVOCs were not able to be synchronously observed. Therefore, future studies should  
527 take into account those BVOCs. Additionally, the uncertainty analysis conducted in this study  
528 indicates the significance of synchronous and accurate observation of photolysis rates and NO<sub>2</sub>  
529 concentration when using the OBM. Generally, this study underlines the significant role of  
530 isoprene chemistry in radical chemistry, photochemical reactions, and secondary pollutant  
531 formation in the atmosphere of the YRD region and provides insights into secondary pollution  
532 and its formation mechanisms.

533

534 *Data availability.* The data that support the results are available from the corresponding author  
535 upon request.

536

537 *Authorship contribution.* Kun Zhang: Formal analysis, Methodology, Writing-original draft.  
538 Ling Huang: Writing-review. Qing Li: Formal analysis. Juntao Huo: Formal analysis, Data  
539 curation. Yusen Duan: Formal analysis, Data curation. Yuhang Wang: Writing-review. Elly  
540 Yaluk: Formal analysis. Yangjun Wang: Formal analysis. Qingyan Fu: Formal analysis. Li Li:  
541 Conceptualization, Methodology, Writing-review & editing.

542

543 *Competing interest.* The authors declare that they have no known competing financial interests  
544 or personal relationships that could have appeared to influence the word reported in this paper.

545

546 *Acknowledgements.* This study is supported by the National Natural Science Foundation of  
547 China (No. 42075144; No.41875161), Shanghai International Science and Technology  
548 Cooperation Fund (No. 19230742500), Shanghai Science and Technology Fund (No.  
549 19DZ1205007), Shanghai Sail Program (NO.19YF1415600), and the National Key Research  
550 and Development Program of China (NO.2018YFC0213600). Y. Wang was supported by the  
551 National Science Foundation. We thank Shanghai Environmental Monitoring Center (SEMC)  
552 for conducting the measurement and sharing the data.

553

554

555 *Financial support.* This study was financially supported by the National Natural Science  
556 Foundation of China (NO. 41875161; NO.42075144), Shanghai International Science and  
557 Technology Cooperation Fund (NO. 19230742500), Shanghai Science and Technology Fund  
558 (No. 19DZ1205007), Shanghai Sail Program (NO.19YF1415600), and the National Key  
559 Research and Development Program of China (NO.2018YFC0213600). Y. Wang was  
560 supported by the National Science Foundation.

561

562 **References**

563 Atkinson, R., and Arey, J.: Atmospheric degradation of volatile organic compounds, Chemical  
564 reviews, 103, 4605-4638, 2003.

565 Atkinson, R., Baulch, D. L., Cox, R. A., Crowley, J. N., Hampson, R. F., Hynes, R. G., Jenkin,  
566 M. E., Rossi, M. J., and Troe, J.: Evaluated kinetic and photochemical data for atmospheric  
567 chemistry: Volume II - Gas phase reactions of organic species, Atmospheric Chemistry and  
568 Physics, 6, 3625-4055, 10.5194/acp-6-3625-2006, 2006.

569 Chan, K. L., Wang, S. S., Liu, C., Zhou, B., Wenig, M. O., and Saiz-Lopez, A.: On the  
570 summertime air quality and related photochemical processes in the megacity Shanghai,  
571 China, Science of the Total Environment, 580, 974-983, 2017.

572 D'Ambro, E. L., Møller, K. H., Lopez-Hilfiker, F. D., Schobesberger, S., Liu, J., Shilling, J.  
573 E., Lee, B. H., Kjaergaard, H. G., and Thornton, J. A.: Isomerization of second-generation  
574 isoprene peroxy radicals: Epoxide formation and implications for secondary organic aerosol  
575 yields, Environmental science & technology, 51, 4978-4987, 2017.

576 Gong, D., Wang, H., Zhang, S., Wang, Y., Liu, S. C., Guo, H., Shao, M., He, C., Chen, D., He,  
577 L., Zhou, L., Morawska, L., Zhang, Y., and Wang, B.: Low-level summertime isoprene  
578 observed at a forested mountaintop site in southern China: implications for strong regional  
579 atmospheric oxidative capacity, Atmospheric Chemistry and Physics, 18, 14417-14432,  
580 10.5194/acp-18-14417-2018, 2018.

581 He, Z. R., Wang, X. M., Ling, Z. H., Zhao, J., Guo, H., Shao, M., and Wang, Z.: Contributions  
582 of different anthropogenic volatile organic compound sources to ozone formation at a  
583 receptor site in the Pearl River Delta region and its policy implications, Atmospheric  
584 Chemistry and Physics, 19, 8801-8816, 2019.

585 Jenkin, M. E., Young, J. C., and Rickard, A. R.: The MCM v3.3.1 degradation scheme for  
586 isoprene, *Atmospheric Chemistry and Physics*, 15, 11433-11459, 10.5194/acp-15-11433-  
587 2015, 2015.

588 Li, X., Rohrer, F., Brauers, T., Hofzumahaus, A., Lu, K., Shao, M., Zhang, Y. H., and Wahner,  
589 A.: Modeling of HCHO and CHOCHO at a semi-rural site in southern China during the  
590 PRIDE-PRD2006 campaign, *Atmospheric Chemistry and Physics*, 14, 12291-12305,  
591 10.5194/acp-14-12291-2014, 2014.

592 Li, Y., Shao, M., Lu, S., Chang, C. C., and Dasgupta, P. K.: Variations and sources of ambient  
593 formaldehyde for the 2008 Beijing Olympic games, *Atmospheric Environment*, 44, 2632-  
594 2639, 10.1016/j.atmosenv.2010.03.045, 2010.

595 Li, L., An, J. Y., Yan, R. S., Huang, C., Wang, H. L., Lou, S. R., Huang, L., Yarwood, G.  
596 Ozone source apportionment over the Yangtze River Delta region, China: Investigation of  
597 regional transport, sectoral contributions and seasonal differences. *Atmospheric  
598 Environment*, 202, 269-280, 2019.

599 Li, L., An, J. Y., Shi, Y. Y., Zhou, M., Yan, R. S., Huang, C., Wang, H. L., Lou, S. R., Wang,  
600 Q., Lu, Q., Wu, J. Source apportionment of surface ozone in the Yangtze River Delta, China  
601 in the summer of 2013. *Atmospheric Environment*, 144, 194-207, 2016.

602 Lin, H., Wang, M., Duan, Y., Fu, Q., Ji, W., Cui, H., Jin, D., Lin, Y., and Hu, K.: O<sub>3</sub> sensitivity  
603 and contributions of different nmhc sources in O<sub>3</sub> formation at urban and suburban sites in  
604 Shanghai, *Atmosphere*, 11, 1-18, 10.3390/atmos11030295, 2020.

605 Liu, X., Lyu, X., Wang, Y., Jiang, F., and Guo, H.: Intercomparison of O<sub>3</sub> formation and radical  
606 chemistry in the past decade at a suburban site in Hong Kong, *Atmospheric Chemistry and  
607 Physics*, 19, 5127-5145, 10.5194/acp-19-5127-2019, 2019.

608 Liu, Y. J., Herdlinger-Blatt, I., McKinney, K. A., and Martin, S. T.: Production of methyl vinyl  
609 ketone and methacrolein via the hydroperoxyl pathway of isoprene oxidation, *Atmospheric*  
610 *Chemistry and Physics*, 13, 5715-5730, 10.5194/acp-13-5715-2013, 2013.

611 Liu, Z., Wang, Y., Gu, D., Zhao, C., Huey, L. G., Stickel, R., Liao, J., Shao, M., Zhu, T., Zeng,  
612 L., Amoroso, A., Costabile, F., Chang, C. C., and Liu, S. C.: Summertime photochemistry  
613 during CAREBeijing-2007: RO<sub>x</sub> budgets and O<sub>3</sub> formation, *Atmospheric Chemistry and*  
614 *Physics*, 12, 7737-7752, 2012.

615 Riedel, T. P., Wolfe, G. M., Danas, K. T., Gilman, J. B., Kuster, W. C., Bon, D. M., Vlasenko,  
616 A., Li, S.-M., Williams, E. J., Lerner, B. M., Veres, P. R., Roberts, J. M., Holloway, J. S.,  
617 Lefer, B., Brown, S. S., and Thornton, J. A. (2014). An MCM modeling study of nitryl  
618 chloride (ClNO<sub>2</sub>) impacts on oxidation, ozone production and nitrogen oxide partitioning in  
619 polluted continental outflow, *Atmos. Chem. Phys.*, 14, 3789–3800,  
620 <https://doi.org/10.5194/acp-14-3789-2014>.

621 Tan, Z. F., Lu, K. D., Jiang, M. Q., Su, R., Wang, H. L., Lou, S. R., Fu, Q. Y., Zhai, C. Z., Tan,  
622 Q. W., Yue, D. L., Chen, D. H., Wang, Z. S., Xie, S. D., Zeng, L. M., and Zhang, Y. H.:  
623 Daytime atmospheric oxidation capacity in four Chinese megacities during the  
624 photochemically polluted season: a case study based on box model simulation, *Atmospheric*  
625 *Chemistry and Physics*, 19, 3493-3513, 2019.

626 Wennberg, P. O., Bates, K. H., Crounse, J. D., Dodson, L. G., McVay, R. C., Mertens, L. A.,  
627 Nguyen, T. B., Praske, E., Schwantes, R. H., Smarte, M. D., St Clair, J. M., Teng, A. P.,  
628 Zhang, X., and Seinfeld, J. H.: Gas-phase reactions of isoprene and its major oxidation  
629 products, *Chemical Reviews*, 118, 3337-3390, 2018.

630 Wolfe, G. M., Kaiser, J., Hanisco, T. F., Keutsch, F. N., de Gouw, J. A., Gilman, J. B., Graus,  
631 M., Hatch, C. D., Holloway, J., Horowitz, L. W., Lee, B. H., Lerner, B. M., Lopez-Hilfiker,  
632 F., Mao, J., Marvin, M. R., Peischl, J., Pollack, I. B., Roberts, J. M., Ryerson, T. B.,

633 Thornton, J. A., Veres, P. R., and Warneke, C.: Formaldehyde production from isoprene  
634 oxidation across NO<sub>x</sub> regimes, *Atmospheric Chemistry and Physics*, 16, 2597-2610,  
635 10.5194/acp-16-2597-2016, 2016a.

636 Wolfe, G. M., Marvin, M. R., Roberts, S. J., Travis, K. R., and Liao, J.: The Framework for 0-  
637 D Atmospheric Modeling (F0AM) v3.1, *Geoscientific Model Development*, 9, 3309-3319,  
638 10.5194/gmd-9-3309-2016, 2016b.

639 Xu, Z., Wang, T., Xue, L. K., Louie, P. K. K., Luk, C. W. Y., Gao, J., Wang, S. L., Chai, F. H.,  
640 and Wang, W. X.: Evaluating the uncertainties of thermal catalytic conversion in measuring  
641 atmospheric nitrogen dioxide at four differently polluted sites in China, *Atmos. Environ.*,  
642 76, 221–226, 2013.

643 Xue, L., Wang, T., Gao, J., Ding, A., Zhou, X., Blake, D. R., Fang, X., Saunders, S. M., Fan,  
644 S., Zuo, H., Zhang, Q., Wang, W. Ground-level ozone in four Chinese cities: precursors,  
645 regional transport and heterogeneous processes. *Atmospheric chemistry and physics*, 14(23),  
646 13175-13188, 2014.

647 Xue, L., Gu, R., Wang, T., Wang, X., Saunders, S., Blake, D., Louie, P. K. K., Luk, C. W. Y.,  
648 Simpson, I., Xu, Z., Wang, Z., Gao, Y., Lee, S., Mellouki, A., and Wang, W.: Oxidative  
649 capacity and radical chemistry in the polluted atmosphere of Hong Kong and Pearl River  
650 Delta region: Analysis of a severe photochemical smog episode, *Atmospheric Chemistry  
651 and Physics*, 16, 9891-9903, 10.5194/acp-16-9891-2016, 2016.

652 Yang, X., Xue, L. K., Wang, T., Wang, X. F., Gao, J., Lee, S. C., Blake, D. R., Chai, F. H., and  
653 Wang, W. X.: Observations and explicit modeling of summertime carbonyl formation in  
654 Beijing: identification of key precursor species and their impact on atmospheric oxidation  
655 chemistry, *Journal of Geophysical Research: Atmospheres*, 123, 1426-1440, 2018.

656 Yang, X., Zhang, G. Q., Sun, Y. M., Zhu, L., Wei, X. F., Li, Z., and Zhong, X. L.: Explicit  
657 modeling of background HCHO formation in southern China, *Atmospheric Research*, 240,  
658 UNSP 10494110.1016/j.atmosres.2020.104941, 2020.

659 Zeng, P., Lyu, X. P., Guo, H., Cheng, H. R., Wang, Z. W., Liu, X. F., and Zhang, W. H.: Spatial  
660 variation of sources and photochemistry of formaldehyde in Wuhan, Central China,  
661 *Atmospheric Environment*, 214, 2019.

662 Zhang, K., Zhou, L., Fu, Q., Yan, L., Bian, Q., Wang, D., and Xiu, G.: Vertical distribution of  
663 ozone over Shanghai during late spring: A balloon-borne observation, *Atmospheric*  
664 *environment*, 208, 48-60, 2019.

665 Zhang, K., Li, L., Huang, L., Wang, Y., Huo, J., Duan, Y., Wang, Y., and Fu, Q.: The impact  
666 of volatile organic compounds on ozone formation in the suburban area of Shanghai,  
667 *Atmospheric Environment*, 232, 10.1016/j.atmosenv.2020.117511, 2020a.

668 Zhang, K., Xu, J., Huang, Q., Zhou, L., Fu, Q., Duan, Y., and Xiu, G.: Precursors and potential  
669 sources of ground-level ozone in suburban Shanghai, *Frontiers of Environmental Science*  
670 and *Engineering*, 14, 10.1007/s11783-020-1271-8, 2020b.

671 Zhu, J., Cheng, H., Peng, J., Zeng, P., Wang, Z., Lyu, X., and Guo, H.: O<sub>3</sub> photochemistry on  
672 O<sub>3</sub> episode days and non-O<sub>3</sub> episode days in Wuhan, Central China, *Atmospheric*  
673 *Environment*, 223, 10.1016/j.atmosenv.2019.117236, 2020a.

674 Zhu, J., Wang, S. S., Wang, H. L., Jing, S. G., Lou, S. R., Saiz-Lopez, A., and Zhou, B.:  
675 Observationally constrained modeling of atmospheric oxidation capacity and  
676 photochemical reactivity in Shanghai, China, *Atmospheric Chemistry and Physics*, 20,  
677 1217-1232, 2020b.

678 Zong, R. H., Yang, X., Wen, L., Xu, C. H., Zhu, Y. H., Chen, T. S., Yao, L., Wang, L. W.,  
679 Zhang, J. M., Yang, L. X., Wang, X. F., Shao, M., Zhu, T., Xue, L. K., and Wang, W. X.:  
680 Strong ozone production at a rural site in the North China Plain: Mixed effects of urban

681 plumes and biogenic emissions, Journal of Environmental Sciences, 71, 261-270,

682 10.1016/j.jes.2018.05.003, 2018.

683